Brain, Behavior, & Immunity - Health 17 (2021) 100336

Contents lists available at ScienceDirect

Brain, Behavior, & Immunity - Health

journal homepage: www.editorialmanager.com/bbih/default.aspx

Full Length Article

A pilot [^{11}C]PBR28 PET/MRI study of neuroinflammation and neurodegeneration in chronic stroke patients

Judith D. Schaechter *, Baileigh G. Hightower, Minhae Kim, Marco L. Loggia

Athinoula A. Martinos Center for Biomedical Imaging Department of Radiology, Massachusetts General Hospital, Harvard Medical School, 13th Street, Building 149, Room 2301, Charlestown, MA, 02129, USA

ARTICLE INFO

Keywords:
TSPO
Activated glia
Microglia
Middle cerebral artery
Ischemia

ABSTRACT

Neuroinflammation occurs in response to acute ischemic stroke, and has been speculated to underlie secondary poststroke pathologies, such as depression, that often develop over time poststroke. However, no study has examined whether neuroinflammation is present in chronic stroke patients (e.g., ≥ 1 year poststroke). This study tested whether neuroinflammation is present in chronic stroke patients, and is associated with neurodegeneration, using [^{11}C]PBR28 PET and diffusion MRI.

Eight patients with middle cerebral artery (MCA) ischemic stroke incurred 1–3 years prior and 16 healthy controls underwent [^{11}C]PBR28 PET to measure glial activation and diffusion MRI to measure microstructural integrity by mean diffusivity (MD) and fractional anisotropy (FA) using an integrated PET/MRI scanner. Group differences in [^{11}C]PBR28 binding, MD and FA were analyzed voxelwise across the whole brain excluding the infarct zone defined as voxels containing the infarct in any patient.

Compared to controls, patients showed elevations in [^{11}C]PBR28 binding in several brain regions outside the infarct zone, including regions with presumed direct neuroanatomical connections to the infarct (e.g., ipsilesional internal capsule and thalamus) and those without known direct connections (e.g., contralesional thalamus and cingulate gyrus). Patients also showed widespread elevations in MD, with a subset of these regions having reduced FA. In patients, MD was more elevated in regions with co-localized elevations in [^{11}C]PBR28 binding than in contralateral regions without elevations in [^{11}C]PBR28 binding.

This pilot study supports the presence of extensive glial activation along with widespread loss in microstructural integrity in non-infarcted tissue in a cohort of patients with chronic MCA stroke. The loss in microstructural integrity was greater in regions with co-localized glial activation. It is possible that stroke risk factors (e.g., hypertension) contributed to these tissue changes in patients.

1. Introduction

Acute ischemic stroke is known to trigger a strong inflammatory response in the infarct core and peri-infarct tissue that involves activation of resident microglia and astrocytes, together referred to as glial activation, and infiltration of peripheral immune cells (Myers et al., 1991a; Rojas et al., 2007; Sette et al., 1993). Over the subsequent weeks poststroke, the neuroinflammatory response in the infarct region wanes (Gulyas et al., 2012; Hughes et al., 2012; Price et al., 2006; Sette et al., 1993), while preclinical stroke studies have shown that glial activation develops in non-infarcted regions connected by white matter to the stroke-damaged tissue (Arlicot et al., 2010; Myers et al., 1991b; Nowicka et al., 2008; Walberer et al., 2014; Walter et al., 2015). In patient case studies, elevated levels of the 18 kDa translocator protein (TSPO), a mitochondrial protein upregulated in activated glia and considered a marker of neuroinflammation, have been observed in non-infarcted tissue weeks to months after middle cerebral artery (MCA) ischemic stroke, most frequently in the ipsilesional thalamus (Gerhard et al., 2005; Pappata et al., 2000; Radlinska et al., 2009; Thiel et al., 2010). While neuroinflammation in chronic stroke patients has been speculated to underlie secondary poststroke pathologies such as depression, fatigue and accelerated age-related cognitive decline that often develop over time poststroke (Barritt and Smithard, 2011; Shi et al., 2019; Spalletta et al., 2006), no study has examined neuroinflammation in a cohort of chronic stroke patients (e.g., ≥1 year poststroke).

The primary aim of this pilot study was to test the hypothesis that neuroinflammation is present in chronic stroke patients. To address this aim, using the TSPO radioligand [^{11}C]PBR28 and an integrated PET/MRI

* Corresponding author.
E-mail address: jschaechter@mgh.harvard.edu (J.D. Schaechter).

https://doi.org/10.1016/j.bbih.2021.100336
Received 29 April 2021; Received in revised form 18 August 2021; Accepted 21 August 2021
Available online 24 August 2021

scanner, we measured glial activation in patients with MCA stroke incurred 1–3 years prior compared to healthy controls in brain tissue undamaged by the stroke in any patient. Furthermore, as several previous studies in MCA stroke subjects have observed secondary neurodegeneration in the thalamus (Justicia et al., 2008; Kuchcinski et al., 2017; Ogawa et al., 1997; Walberer et al., 2014; Walter et al., 2015), a region that has also been observed to be affected by neuroinflammation after MCA stroke, our secondary aim was to examine whether neurodegeneration (e.g., Wallerian degeneration, secondary neurodegeneration) accompanied neuroinflammation in chronic patients with MCA stroke. To address this aim, microstructural integrity of brain tissue undamaged by stroke was measured by mean diffusivity (MD) and fractional anisotropy (FA) based on diffusion MRI.

2. Materials and methods

2.1. Study design

This study was conducted at the Athinoula A. Martinos Center for Biomedical Imaging, Massachusetts General Hospital. The Institutional Review Board and Radioactive Drug Research Committee approved the protocol. All subjects gave written informed consent.

2.2. Participants

Eight patients completed the study, and 16 healthy controls who participated in other PET/MRI studies (led by investigator MLL) were selected to match the patient group in age, sex, and Ala147Thr TSPO genotype. Inclusion criterion for patients was a unilateral ischemic stroke in the MCA territory 1–3 years prior. Exclusion criteria for patients were significant cognitive deficit measured by NIH Stroke Scale (NIHSS) item 1b and 1c score $\geq$1 or NIHSS item 9 score $\geq$2 (Brott et al., 1989); significant pre-stroke disability measured by the modified Rankin Scale score $\geq$3 (scale 0–5) (Bruno et al., 2011); and significant pre-stroke fatigue measured by verbal rating score >3 (scale 0–10). Exclusion criteria for patients and controls were a PET/MRI contraindication (e.g., certain metallic implants, claustrophobia); neurological disorder (other than chronic stroke in patients); and major kidney or liver disease. Enrolled subjects were subsequently excluded from imaging due to use of a benzodiazepine with high TSPO binding affinity (e.g., diazepam) or systemically-acting immunomodulator (e.g., prednisone) within 2 weeks of scheduled PET/MRI; active infection at time of scheduled PET/MRI; or Thr/Thr genotype in Ala147Thr TSPO gene that predicts low affinity binding of [^{11}C]PBR28 (Owen et al., 2012).

Patients were characterized with regard to motor function using the upper limb subtest of the Fugl-Meyer Stroke Scale (FMSS-UL) that scales from 0 to 60, indicating poor to good motor recovery of the upper limb (Woodbury et al., 2007), and the 10-Meter Walk Test (10MWT) that measures comfortable walking speed (Flansbjer et al., 2005). As a normative reference for the 10MWT, community ambulation requires walking speed $\geq$0.8 m/s (Middleton et al., 2015). Fatigue was characterized using the general fatigue subtest of the Multidimensional Fatigue Inventory (MFI) that scales from 4 to 20, indicating low to high fatigue (Smets et al., 1995). Depression was characterized using the depression subtest of the Hospital Anxiety and Depression Scale (HADS-D) that scales from 0 to 21, indicating low to high depression (Zigmond and Snaith, 1983).

2.3. Image acquisition

Images were acquired using an integrated PET/MRI scanner that consists of a brain avalanche photodiode-based PET scanner operating in the bore of a Siemens 3T Tim Trio MRI and allows for simultaneous acquisition of PET and MRI data (Kolb et al., 2012). [^{11}C]PBR28 scans were acquired 60–90 min after intravenous bolus injection of [^{11}C]PBR28 and stored in listmode format. T1-weighted images (repetition time (TR) 2.53 s; echo time (TE)$_{1\text{-}4}$ 1.63/3.49/5.35/7.21 ms; voxel size 1 $\times$ 1 $\times$ 1 mm) were acquired from all subjects. Fluid-attenuated inversion recovery (FLAIR) images (TR 10 s; TE 73 ms; voxel size 1.3 $\times$ 1.0 $\times$ 5.0 mm) were acquired from patients. Diffusion MRI was performed on 7 of 8 patients and 11 of 16 controls using a twice-refocused echo planar spin-echo sequence (TR 8 s; TE 119 ms; voxel size 2.5 $\times$ 2.5 $\times$ 2.5 mm; 60 diffusion weightings at b-value 3000 s/mm^2 and 8 at b-value 0 s/mm^2).

2.4. Image analysis

PET data were reconstructed using the three-dimensional Ordinary Poisson Ordered Subset Expectation Maximization algorithm from prompt and random coincidences, normalization, attenuation, and scatter coincidence sinograms using 32 subsets and 1 iteration. A statistical parametric mapping-based, pseudo-computed tomography methodology was used to conduct MR-based attenuation correction (Izquierdo-Garcia et al., 2014). Standardized uptake value (SUV) images were calculated (i.e., radioactivity concentration divided by injected dose per body weight) from the 60–90 min post-administration [^{11}C]PBR28 PET data and processed as we described previously (Albrecht et al., 2018; Loggia et al., 2015). SUV images were spatially normalized to Montreal Neurological Institute (MNI) space using tools in the FMRIB's Software Library (FSL, version 6). SUV images from patients with a left hemisphere stroke (3 of 8 patients) were flipped across the midsagittal plane prior to spatial normalization to lateralize the infarct to the right hemisphere for all patients. Each patient's infarct was labeled on the T1-weighted images, aided by visualizing the infarct on the FLAIR images as needed. This lesion label was used to measure lesion volume and to mask out the infarct during the spatial normalization process (Brett et al., 2001). Spatially normalized SUV images were smoothed with an 8 mm full width at half maximum (FWHM) Gaussian kernel.

To account for global differences in [^{11}C]PBR28 binding across individuals, we normalized SUV images by signal in a pseudo-reference region, yielding SUVR images (Albrecht et al., 2018), with the ipsilesional (right) cerebellum serving as the pseudo-reference region. Several prior TSPO PET studies in MCA stroke patients have used the ipsilesional cerebellum as the pseudo-reference region because this region is spared effects of diaschisis (Gerhard et al., 2005; Gulyas et al., 2012; Morris et al., 2018; Price et al., 2006). We assessed the suitability of the ipsilesional cerebellum as the pseudo-reference region for our data, with the criterion begin the absence of a significant ($p < 0.05$) difference in mean SUV in the right cerebellum of patients compared to controls, with the cerebellum defined by the probabilistic cerebellar label in FSL's MNI Structural Atlas (thresholded at 50, range 0–100). We found no significant between-group difference in right cerebellar SUV after adjusting for TSPO genotype and age, supporting the suitability of the right cerebellum as the pseudo-reference region when the statistical model to assess group differences in SUVR adjusts for TSPO genotype and age.

The diffusion MRI data were processed using software from FMRIB's Diffusion Toolbox (FDT). These data were corrected for eddy currents and head motion, then the diffusion tensor and associated eigensystem were estimated voxelwise using linear least squares regression, from which MD and FA were calculated. MD is the average of the three eigenvalues and quantifies average diffusivity. FA is the fraction of diffusion attributed to anisotropic diffusion, and scales from 0 indicated isotropy to 1 indicating anisotropy (Basser and Pierpaoli, 1996). Increases in intravoxel MD and decreases in intravoxel FA typically reflect loss in tissue microstructural integrity and have been used as indices of neurodegeneration after stroke (e.g., Wallerian degeneration, secondary neurodegeneration) (Herve et al., 2005; Werring et al., 2000). MD and FA images were spatially normalized to MNI space using the same procedure as for the SUV images, then smoothed with a 4 mm FWHM Gaussian kernel.

To compare [^{11}C]PBR28 binding, MD and FA in the patients relative to controls in MNI space, we sought to exclude all voxels containing an

infarct in any patient. To prepare for this, each patient's lesion label delineated on the T1-weighted images was spatially normalized, then these labels were summed voxelwise to create a cumulative lesion map. The cumulative lesion map was binarized to create a composite lesion map that defined the infarct zone to be excluded in subsequent analyses.

With time after stroke, the size of an infarct typically shrinks, which results in a proportionate increase in size of the ipsilesional lateral ventricle (Egorova et al., 2019). Accordingly, we wished to exclude all lateral ventricle voxels during group comparison of [^{11}C]PBR28 binding, MD and FA in MNI space. In preparation for this, lateral ventricle voxels of each subject were automatically labeled in the T1-weighted images using Freesurfer software, these labels were spatially normalized, summed voxelwise and binarized to create a composite lateral ventricle map.

2.5. Statistical analysis

Statistical differences in demographic variables between patient and control groups were assessed by a two-tailed unpaired *t*-test for continuous data (i.e., age, body weight, molar activity, injected dose, injected dose/body weight), and two-tailed Fisher's Exact test for nominal data (i.e., sex, TSPO genotype, stroke risk factors). Pearson's correlation coefficient was computed to assess the relationship between [^{11}C]PBR28 binding and lesion volume in patients. The difference in [^{11}C]PBR28 binding between patients median-split by stroke chronicity was assessed using a two-tailed unpaired *t*-test. Testing was performed using JMP Pro (v15) software with significance level set at 0.05.

Group differences in [^{11}C]PBR28 binding, MD and FA were evaluated voxelwise by a nonparametric permutation test implemented using FSL's randomize tool with 5000 permutations, with significance level set at 0.05 using threshold-free cluster enhancement (TFCE) (Smith and Nichols, 2009). Voxels of the composite lesion and lateral ventricle maps were excluded from analysis. The model assessing group differences in [^{11}C]PBR28 binding included TSPO genotype and age as regressors of no interest. The model assessing group differences in MD and FA included age as a regressor of no interest because increased age among older adults has been associated with changes in diffusion (Reas et al., 2020; Salat et al., 2005; Salminen et al., 2016), and there was a non-significant trend ($p = 0.053$) for greater age in the patients ($n = 7$) compared to the controls ($n = 11$) with diffusion MRI data.

For the purposes of displaying scatterplots of group differences in [^{11}C]PBR28 binding, MD and FA, for correlating [^{11}C]PBR28 binding against lesion volume in patients, and for testing the difference in [^{11}C]PBR28 binding in patients median-split by stroke chronicity, we computed values adjusted for the effect of covariate(s). To do this, the mean imaging metric across all voxels of interest (corrected $p < 0.05$) was computing for each subject, then these data along with relevant covariate data were entered into a linear regression model in JMP software. Covariates for adjusting [^{11}C]PBR28 binding (SUVR) were TSPO genotype and age, whereas the covariate for adjusting MD and FA was age. This process was repeated for selected regions within the group difference map in [^{11}C]PBR28 binding by intersecting with anatomic labels extracted from FSL's atlases. The selected regions were the right and left thalamus and white matter from the Harvard-Oxford Subcortical Structural Atlas, with each label thresholded at a minimum value of 70 (range 0–100); right precentral gyus from the Harvard-Oxford Cortical Structural Atlas thresholded at a minimum value of 20; right superior longitudinal fasciculus from the Johns Hopkins University (JHU) ICBM-DTI-81 White Matter Tractography Atlas thresholded at a minimum value of 20; and the corpus callosum body and right cerebral peduncle from the JHU ICBM-DTI-81 White Matter Label Atlas.

To further explore our finding of significant group differences in [^{11}C]PBR28 binding and diffusion (see Results), we delineated the spatial overlap between group difference maps (SUVR relative to MD and FA, separately), with the input maps thresholded at corrected p-level < 0.05 and binarized. We then asked if the magnitude of diffusion differed in patients relative to the presence or absence of overlapping group differences in [^{11}C]PBR28 binding. To address this question in such a way that accounts for the normal variability in diffusion across the brain, we constructed symmetric regions-of-interest, with one region-of-interest comprised of voxels with overlapping group differences [^{11}C]PBR28 binding and diffusion and the contralateral region-of-interest comprised of voxels with a group difference in diffusion only. Mean diffusion was calculated for both regions-of-interest for each subject, then these values were entered into a repeated measures mixed model analysis to test for a region-of-interest $\times$ group interaction effect on mean diffusion, with planned post-hoc contrast between diffusion in the two regions-of-interest in patients using the Tukey test. To avoid circularity, the mixed model analyses were not used to test group effects. These statistical analyses were performed using JMP software with significance level set at 0.05.

3. Results

3.1. Subject characteristics

Subject characteristics are shown in Table 1. There was no significant group difference in age, sex or TSPO genotype, reflecting successful selection of controls from an existing dataset. While the dose of [^{11}C]PBR28 was higher in patients than controls, and molar activity was higher in controls than patients, injected dose per body weight was not significantly different between groups, indicating appropriate normalization of brain radioactivity concentration to calculate SUV. Patients had a significantly higher incidence of some stroke risk factors (e.g., hypertension) compared to controls, as might be expected given the high comorbidity of hypertension and stroke. Infarct volume and location within the MCA territory varied across patients (Fig. 1a). The cumulative lesion

Table 1
Subject characteristics.

	Patients	Controls	p-value
Age (y)	62 ± 6	57 ± 7	0.06
Sex (female/total)	1/8	8/16	0.18
TSPO genotype (MAB/total)	2/8	6/16	0.67
Body weight (kg)	83 ± 15	74 ± 19	0.23
Molar activity (GBq/μmol)	51.4 ± 18.8	81.8 ± 31.4	<0.01
Injected dose (mCi)	14.63 ± 0.15	12.69 ± 1.66	<0.01
Injected dose/body weight	0.18 ± 0.04	0.18 ± 0.05	0.96
Stroke Risk Factors			
Hypertension (positive/total)	4/8; 3/7	0/16; 0/11	0.01; 0.04
Hyperlipidemia (positive/total)	4/8; 3/7	1/16; 1/11	0.03; 0.25
Diabetes or pre-diabetes (positive/total)	1/8; 1/7	2/16; 1/11	1.00; 1.00
Coronary artery disease (positive/total)	3/8; 3/7	0/16; 0/11	0.03; 0.04
Atrial fibrillation (positive/total)	0/8; 0/7	0/16; 0/11	–
Stroke Characteristics and Acute Treatment			
Time interval acute stroke to scan (y)	1.7 ± 0.5	–	
Infarct volume (cm^3)	18 ± 17	–	
Hemisphere (right)	5/8	–	
Tissue plasminogen activator (positive/total)	1/8	–	
Intra-arterial therapy (positive/total)	1/8	–	
Patient Clinical Characteristics			
FMSS-UL score (scale 0–60)	59 (40–60)	–	
10MWT (m/s)	1.4 ± 0.2	–	
MFI score (scale 4–20)	10 (5–15)	–	
HADS-D score (scale 0–21)	4 (0–7.5)	–	

Abbreviations: MAB = mixed affinity binder.
Continuous data given as mean and standard deviation; ordinal data given as median and range; nominal data given as count relative to total.
For stroke risk factors: Values given for all subjects and subset of subjects with diffusion MRI data.

map shows partial spatial overlap of the infarcts across patients (Fig. 1b).

The clinical data from the patients indicate that, as a group, they had good upper and lower limb motor function, mild depression and moderate fatigue.

3.2. [^{11}C]PBR28 binding in patients compared to controls

Compared to controls, the patients showed significant elevations in [^{11}C]PBR28 binding in a large volume of brain tissue (109 cm^3 in MNI space) outside the infarct zone, including in regions of the ipsilesional superior corona radiata, ipsilesional supplementary motor area, ipsilesional superior longitudinal fasciculus, ipsilesional internal capsule, contralesional cingulate gyrus, corpus callosum, bilateral thalamus, bilateral midbrain and bilateral pons (Fig. 2; Table 2). There was no region with significantly higher [^{11}C]PBR28 binding in the controls than patients. These findings provide evidence of extensive neuroinflammation in non-infarcted ipsilesional and contralesional regions in chronic stroke patients.

In patients, [^{11}C]PBR28 binding (adjusted for TSPO genotype and age) outside the infarct zone was not significantly correlated with lesion volume ($r = -0.44$, $p = 0.28$). Adjusted [^{11}C]PBR28 binding in the contralesional thalamus, a region with no known direct white matter connections to a stroke in the MCA territory, was not significantly different in patients median-split by stroke chronicity (high chronicity: 1.27 ± 0.05; low chronicity: 1.21 ± 0.08; $p = 0.20$).

3.3. Diffusion in patients compared to controls

Compared to controls, the patients showed significant elevations in MD in a large volume of tissue (551 cm^3 in MNI space) outside the infarct zone, including white matter of the frontal, temporal, parietal and occipital lobes bilaterally, corpus callosum, ipsilesional pallidum, bilateral thalamus, bilateral midbrain and bilateral cerebellum (Fig. 3a). The patients also showed reductions in FA (35 cm^3 in MNI space) outside the infarct zone, in regions of the corpus callosum body, ipsilesional superior longitudinal fasciculus, ipsilesional precentral gyrus, and contralesional cingulate gyrus (Fig. 3c). There was no region with significantly higher MD or lower FA in the controls than patients. The group differences in diffusion provide evidence of widespread loss in microstructural integrity in chronic stroke patients when indexed by elevations in MD, though more spatially restricted microstructural loss when indexed by reductions in FA.

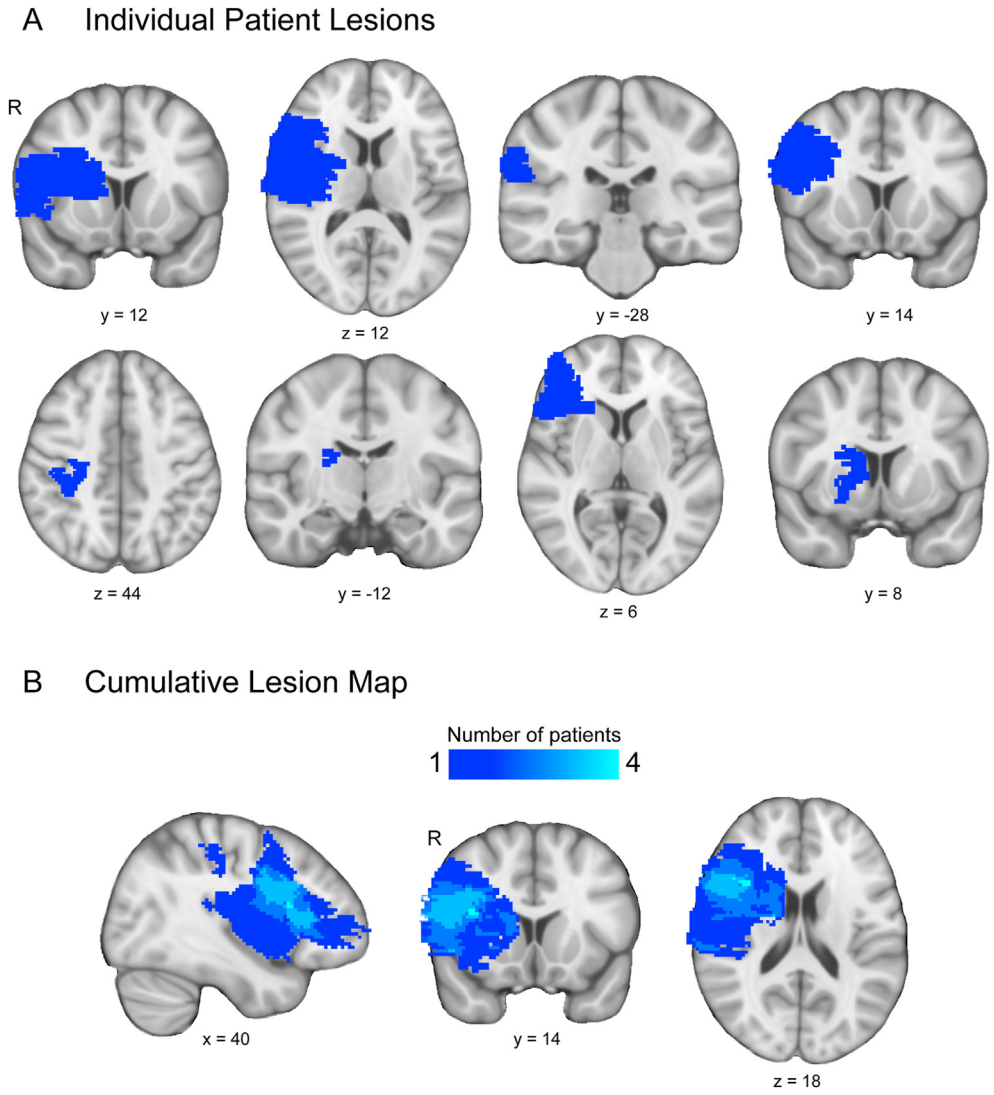

Fig. 1. Location of stroke in MCA territory in patients. All lesions shown in the right hemisphere in MNI space **A.** Slice showing largest lesion extent in each of 8 patients. **B**. Cumulative lesion map in 8 patients. The blue color scale represents the number of patients with a lesion at the voxel location. . (For interpretation of the references to color in this figure legend, the reader is referred to the Web version of this article.)

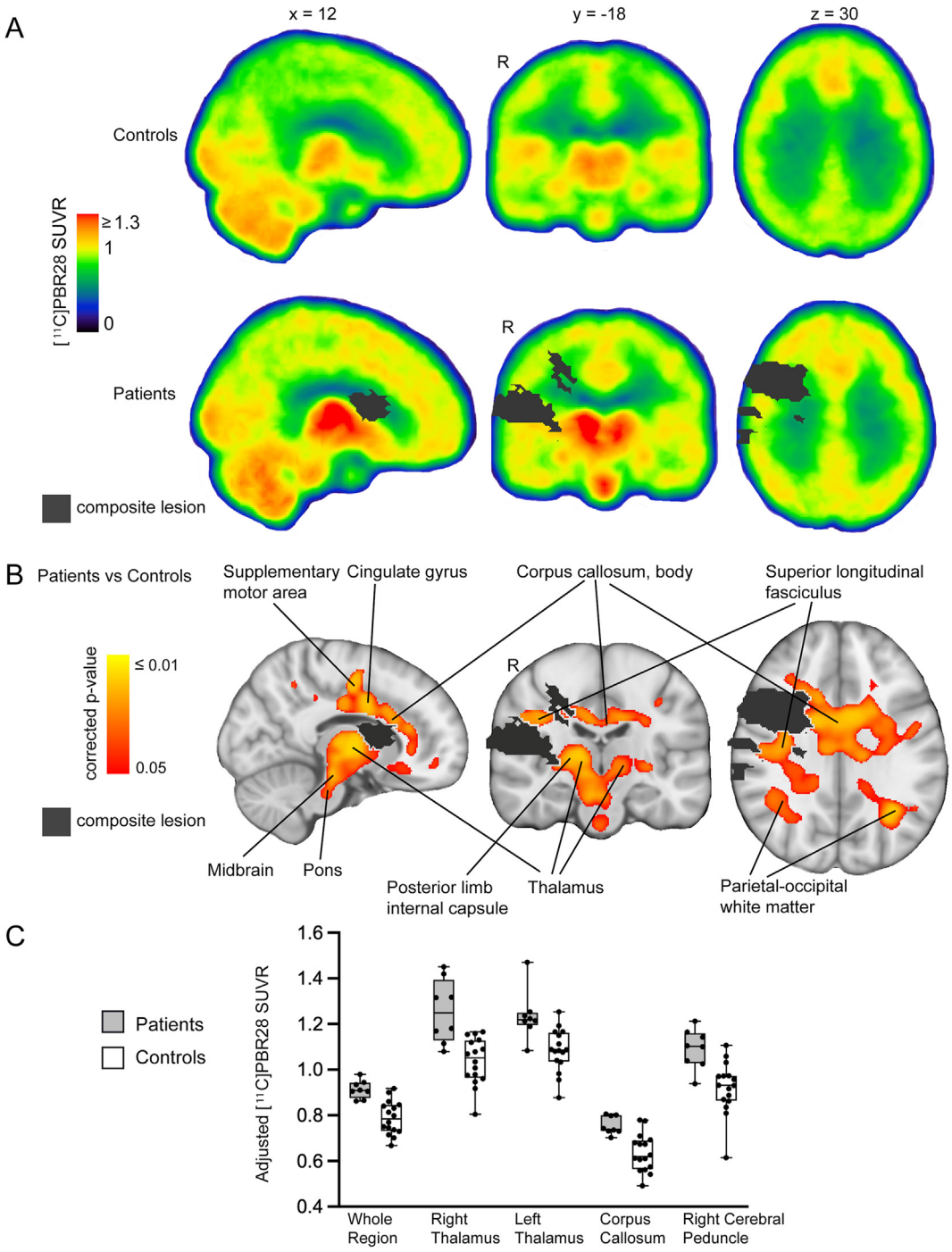

Fig. 2. Evidence of neuroinflammation in stroke patients. **A.** Median [^{11}C]PBR28 SUVR in controls (n = 16) and patients (n = 8). **B.** Brain regions with significant elevations in [^{11}C]PBR28 binding in patients versus controls. **C.** [^{11}C]PBR28 SUVR, adjusted for TSPO genotype and age, for each subject across all voxels exhibiting a significant group difference (whole region), and in selected regions intersecting the group difference map. Adjusted [^{11}C]PBR28 SUVR data are displayed in box-and-whisker plots, with each box extending from 25th to 75th percentile, whiskers extending from minimum and maximum value, and horizontal line representing the median.

3.4. Relationship between group differences [^{11}C]PBR28 binding and diffusion

We next evaluated the spatial overlap between group differences in [^{11}C]PBR28 binding and diffusion. The group difference maps in [^{11}C]PBR28 binding and MD overlapped by 62 cm^3, with 57% of the volume exhibiting an elevation in [^{11}C]PBR28 binding in patients also exhibiting an elevation in MD. The overlap volume involved regions of the ipsilesional superior longitudinal fasciculus, ipsilesional internal capsule, corpus callosum, bilateral cingulate gyrus, bilateral thalamus (ipsilesional more than contralesional), and bilateral midbrain (Fig. 4a). Of note, a large portion of the volume exhibiting an elevation in [^{11}C]PBR28 binding in the patients that did not overlap with an elevation in MD was located in gray matter regions of the thalamus, midbrain and pons bilaterally and the contralesional pallidum (Fig. 4b). The group difference maps in [^{11}C]PBR28 binding and FA overlapped by 8 cm^3, with only 8% of the volume exhibiting an elevation in [^{11}C]PBR28 binding in patients also having a reduction in FA. This overlap volume involved

Table 2
Regions exhibiting significantly higher [^{11}C]PBR28 binding in patients compared to controls.

Cluster size (voxels)	Region within Cluster	Hemisphere	Local Maxima MNI Coordinates (mm)		
			X	Y	Z
8864	Superior corona radiata	Ipsilesional	18	0	38
	Superior longitudinal fasciculus	Ipsilesional	38	−16	32
	Parietal-occipital white matter	Ipsilesional	42	−50	38
	Supplementary motor area	Ipsilesional	12	−8	48
	Corpus callosum, body	Ipsilesional & Contralesional	0	2	24
	Cingulate gyrus	Contralesional	−6	−4	34
	Precentral gyrus	Contralesional	−24	−8	52
3507	Posterior limb of internal capsule	Ipsilesional	16	−8	2
	Thalamus	Ipsilesional & Contralesional	12	−10	2
	Midbrain	Ipsilesional & Contralesional	0	−26	−18
	Pons	Ipsilesional & Contralesional	−2	−32	−38
1375	Parietal-occipital white matter	Contralesional	−32	−60	22
19	Superior precentral white matter	Contralesional	−8	−28	66

regions of the corpus callosum body (anterior more than posterior), ipsilesional superior longitudinal fasciculus, ipsilesional precentral gyurs, and contralesional cingulate gyrus (Fig. 4c). Overall, these findings indicate that a substantial portion of brain tissue showing evidence of neuroinflammation in patients (i.e., elevated [^{11}C]PBR28 binding) co-localized with tissue showing loss in microstructural integrity when indexed by elevated MD, though not when indexed by reduced FA.

We then tested for an interaction between group and region-of-interest (co-localized group differences in [^{11}C]PBR28 binding and diffusion versus group difference in diffusion only) on the magnitude of diffusion (MD and FA, separately). We found a significant interaction between group and region-of-interest on MD ($p < 0.01$, mixed model repeated measures analysis), with MD significantly higher in the patients but not controls in the region-of-interest with group differences in both [^{11}C]PBR28 binding and MD relative to the region-of-interest with a group difference in MD only ($p < 0.001$, Tukey testing; Fig. 5). There was no significant interaction effect between group and region-of-interest on FA. These findings provide evidence that loss in microstructural integrity in patients, indexed by elevated MD, was more severe in brain tissue that also exhibited glial activation.

4. Discussion

The current PET study is the first to demonstrate elevated TSPO binding in non-infarcted tissue in a cohort of patients with chronic (1–3 years) MCA stroke. To our knowledge, our study is also the first to evaluate neuroinflammation in stroke patients using [^{11}C]PBR28, a second generation TSPO radioligand with 80-fold higher specific binding for activated brain glia than [^{11}C]PK11195 (Kreisl et al., 2010), the prototypical TSPO radioligand used in the great majority of prior TSPO PET studies in stroke patients (Gerhard et al., 2005; Morris et al., 2018; Pappata et al., 2000; Price et al., 2006; Radlinska et al., 2009; Thiel et al., 2010). Our findings provide evidence of extensive glial activation in chronic stroke patients, leading to the possibility that chronic neuroinflammation may play a role in secondary poststroke pathologies such as depression and fatigue (Barritt and Smithard, 2011; Shi et al., 2019; Spalletta et al., 2006).

Previous studies in patients and animal models with subacute MCA stroke have observed glial activation in the ipsilesional thalamus and ipsilesional internal capsule, regions with known neuroanatomical connections to the damaged tissue (Arlicot et al., 2010; Gerhard et al., 2005; Justicia et al., 2008; Pappata et al., 2000; Radlinska et al., 2009; Thiel et al., 2010; Walberer et al., 2014; Walter et al., 2015). Case studies of patients who incurred an MCA stroke several months prior have also observed glial activation in more distal connections of the damaged tissue, including in the midbrain and pons (Gerhard et al., 2005; Walter et al., 2015). Consistent with these prior studies, the patients in the current study showed elevations in [^{11}C]PBR28 binding in the ipsilesional thalamus, ipsilesional internal capsule, midbrain and pons. Our patients exhibited elevations in [^{11}C]PBR28 binding in additional regions with presumed connections to damaged tissue, including the ipsilesional superior longitudinal fasciculus, ipsilesional superior corona radiata and corpus callosum body. Notably, our patients also showed elevated [^{11}C]PBR28 binding in regions with no known direct connections to an infarct in the MCA territory, including the contralesional thalamus and contralesional cingulate gyrus. The favorable properties of [^{11}C]PBR28, including higher signal-to-noise binding and higher brain uptake compared to first-generation TSPO radioligands (Briard et al., 2008; Kreisl et al., 2010), likely contributed to us detecting previously unseen TSPO signal in stroke patients. The spatial distribution of elevated [^{11}C]PBR28 binding we observed in the chronic stroke patients might have resulted from spreading of glial activation after MCA stroke, early on involving regions with proximal neuroanatomical connections to the infarct, later involving more distal connections, and also extending transsynaptically to regions without direct connections to damaged tissue. Transsynaptic spread of glial activation to regions with abnormal functional activity has been proposed in models of Huntington Disease (Topper et al., 1993) and epilepsy (Taniwaki et al., 1996). The glial activation we observed in regions without direct structural connections to the infarct zone may have similarly been due to altered functional activity secondary to stroke.

Patients in the current study also showed widespread elevations in MD, and more spatially restricted reductions in FA. Previous studies in MCA stroke subjects have observed elevations in MD and reductions in FA in regions with neuroanatomical connections to damaged tissue, including in the ipsilesional internal capsule, ipsilesional thalamus, and corpus callosum (Buffon et al., 2005; Gupta et al., 2006; Herve et al., 2005; Jason et al., 2011; Liang et al., 2007; Werring et al., 2000). We found the elevations in MD in the patients to be far more widespread than previous reports, and to involve regions both with and without known neuroanatomical connections to an MCA territory infarct, suggesting that factors in addition to stroke contributed to pervasive loss of tissue microstructure.

The higher incidence of hypertension in our patients compared to controls may have contributed to the widespread loss in tissue microstructure. Hypertension has been associated with elevated MD and reduced FA of brain white matter (Gons et al., 2010; Kennedy and Raz, 2009; McEvoy et al., 2015; Salat et al., 2012). Some studies have shown that increases in blood pressure are associated with widespread elevations in MD and more spatially restricted reductions in FA (Maclullich et al., 2009; Maillard et al., 2012), similar to the spatial pattern of diffusion abnormalities we observed in our patients. The presence of multiple vascular risk factors (e.g., hypertension and diabetes) has been shown to amplify MD elevations and FA reductions compared to individual risk factors (Cox et al., 2019). Our observation of widespread MD elevations and more spatially restricted FA reductions in the patients may reflect combined effects of long term neurodegenerative changes due to stroke risk factors and secondary neurodegenerative changes due to stroke.

Our diffusion MRI protocol acquired the diffusion-weighted images at a high b-value (3000 s/mm^2), which is higher than a conventional b-value of 700–1000 s/mm^2. High b-value diffusion MRI (i.e., ≥2000 s/

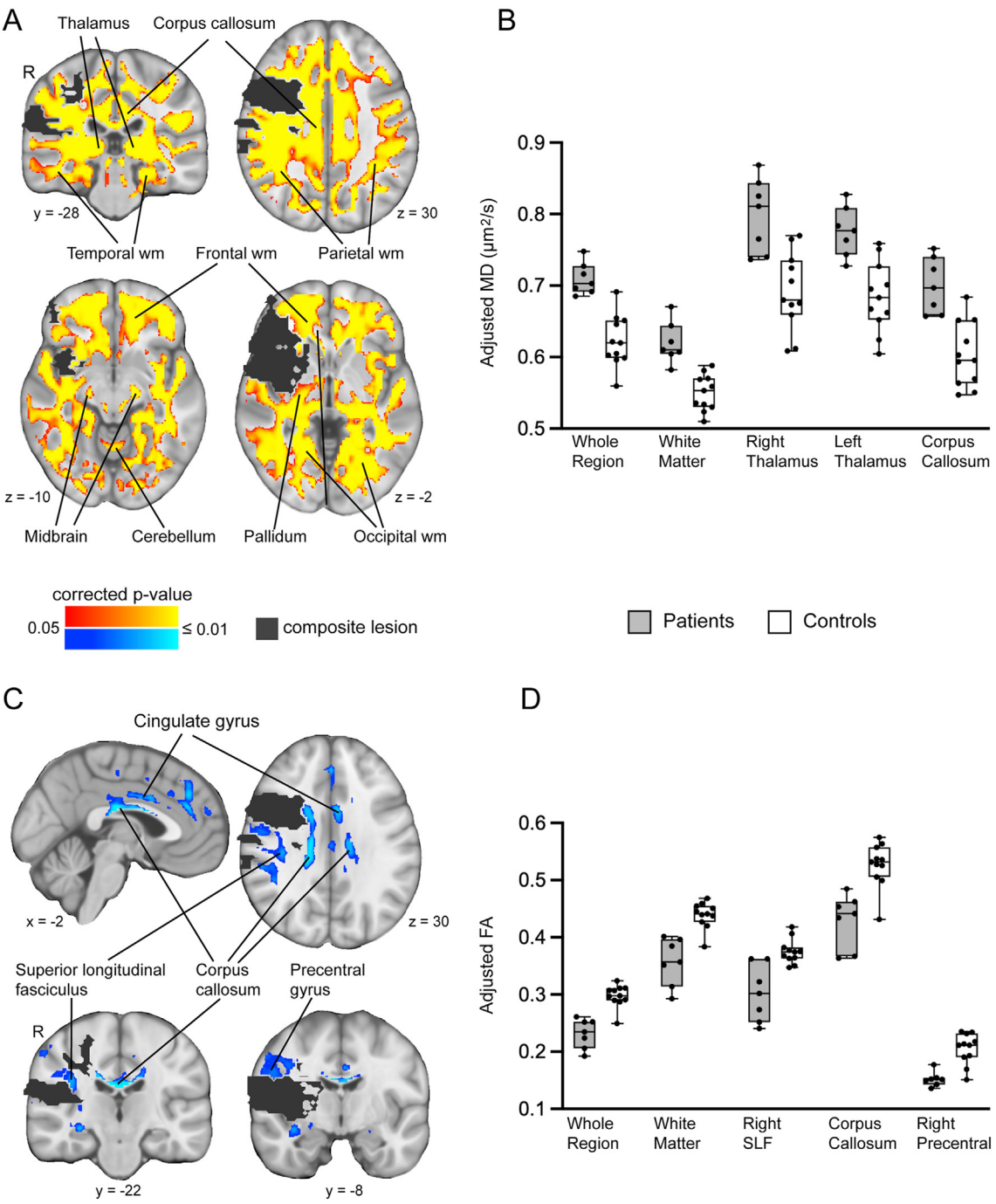

Fig. 3. Evidence of neurodegeneration in patients. **A**. Brain regions with significant elevations in MD in patients relative to controls. wm = white matter**. B**. MD, adjusted for age, for each subject across all voxels exhibiting a significant group difference (whole region), and in selected regions intersecting the group difference map. **C**. Brain regions with significant reductions in FA in patients relative to controls. **D**. FA, adjusted for age, for each subject across all voxels exhibiting a significant group difference (whole region), and in selected regions intersecting the group difference map. Box-and-whisker plots displayed as in Fig. 2.

mm^2) has been shown to improve the sensitivity to detect differences in diffusivity (measured by MD or apparent diffusion coefficient, ADC) in several patient populations compared to conventional b-value diffusion MRI (Baumann et al., 2012; Hyare et al., 2010; Shiraishi et al., 2005; Yoshiura et al., 2003), while not conferring improved sensitivity to differences in FA (Baumann et al., 2012; Hagmann et al., 2010). Biophysical modeling suggests that high b-value diffusion MRI increases the proportion of signal coming from a slow-diffusing compartment, whereas conventional b-value diffusion MRI detects signal mostly from a fast-diffusing compartment (Assaf and Cohen, 2000). The slow-diffusing compartment is highly restricted and thought to represent movement of water within axons or between myelin membranes (Assaf and Cohen, 2000). Taken together, the widespread elevations in MD observed in patients relative to controls revealed using high b-value diffusion MRI may represent diffuse axonal pathology due to longstanding effects of stroke risk factors.

A substantial portion (57%) of brain tissue showing an elevation in [^{11}C]PBR28 binding in patients also showed an elevation in MD. This finding is consistent with prior immunohistochemical studies in animal models of stroke (Justicia et al., 2008; Schroeter et al., 1999) and imaging studies in stroke patients (Thiel et al., 2010) indicating co-localization of neuroinflammation and neurodegenerative changes

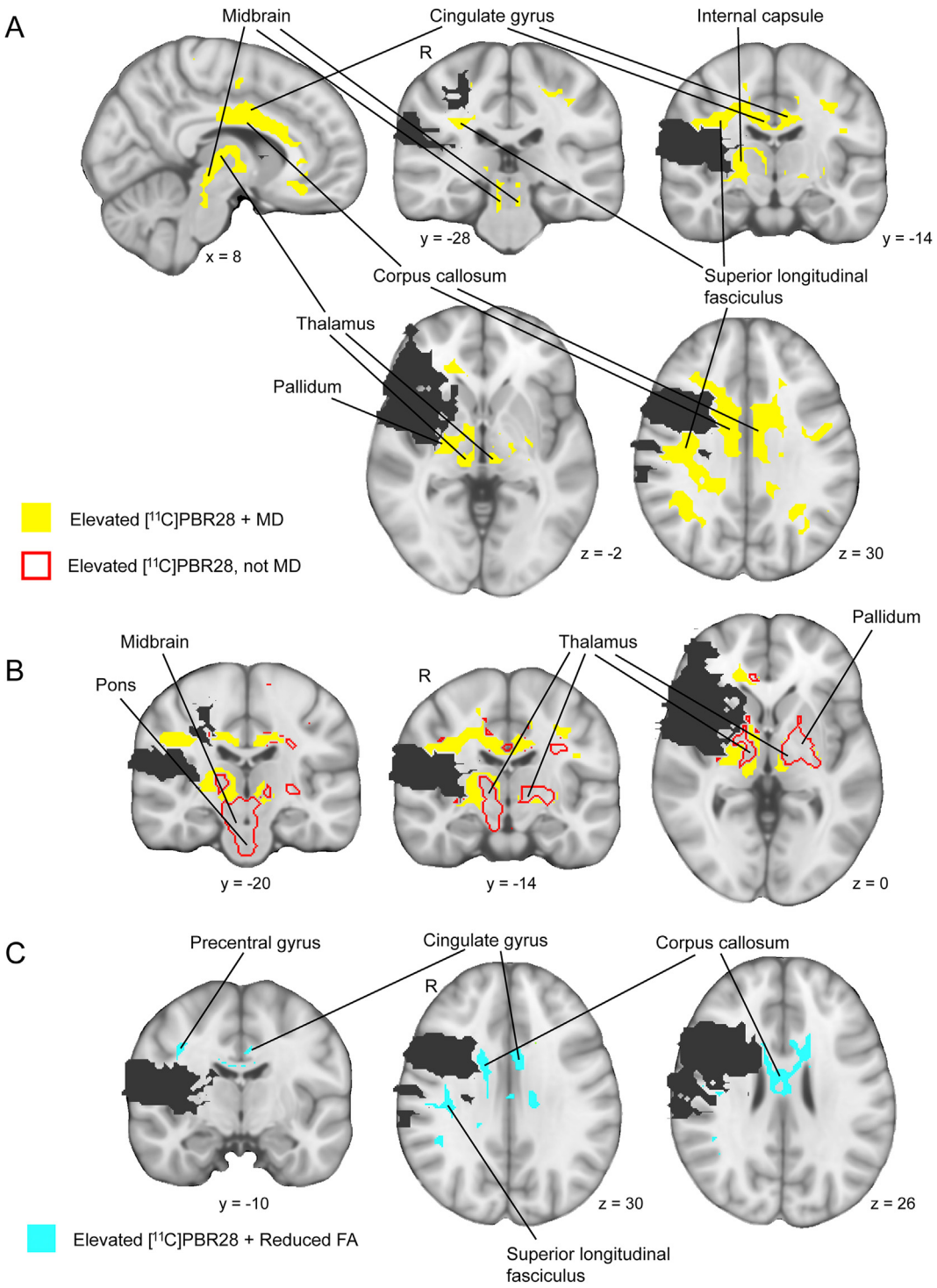

Fig. 4. Spatial relationship between brain regions with evidence of group differences in [^{11}C]PBR28 binding and diffusion. **A**. Brain regions with overlapping elevations in [^{11}C]PBR28 binding and MD in patients (yellow areas). **B**. Brain regions with an elevation in [^{11}C]PBR28 binding in patients unaccompanied by an elevation in MD (areas outlined in red). **C**. Brain regions with elevations in [^{11}C]PBR28 binding in patients overlapping reductions in FA in patients (aqua areas). (For interpretation of the references to color in this figure legend, the reader is referred to the Web version of this article.)

after stroke. Notably, we also observed that substantial portions of subcortical gray matter (e.g., thalamus, midbrain, pons) that showed elevations in [^{11}C]PBR28 binding in patients did not also show elevations in MD. At face value, this result might represent non-infarcted tissue with neuroinflammation but not neurodegeneration. However, it is also possible that microstructural loss in these subcortical gray matter regions was underestimated due to use of high b-value diffusion MRI that is particularly sensitive to axonal pathology, and less sensitive to gray matter pathology (Assaf et al., 2003). Future studies that utilize multi-shell diffusion MRI analyzed using a non-Gaussian model of water diffusion, an approach demonstrating gray matter neurodegeneration in other studies (Fukutomi et al., 2019; Vogt et al., 2020), may help clarify the extent of co-localized neuroinflammation and neurodegeneration in gray matter in chronic stroke patients.

Patients were found to have a greater elevation in MD in voxels that also exhibited an elevation in [^{11}C]PBR28 binding compared to voxels

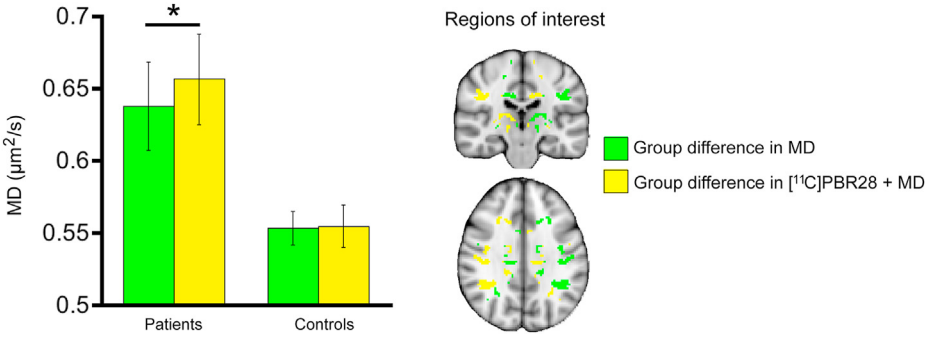

Fig. 5. Greater elevation in MD in regions with co-localized elevations in [^{11}C]PBR28 binding. Mean MD (±standard deviation) is shown for patients and controls in a region-of-interest with group differences in both [^{11}C]PBR28 binding and MD, and the contralateral region-of-interest with a group difference in MD only. A significant interaction between group and region-of-interest on MD was found ($p < 0.01$, mixed model repeated measures analysis), with MD greater in patients, and not controls, in the region-of-interest with co-localized group differences in [^{11}C]PBR28 binding and MD compared the region-of-interest with a group difference in MD only (*$p < 0.001$, Tukey testing).

exhibiting an elevation in MD only. While it is recognized that activated glia can have either neurorestorative or neurodegenerative functions depending on time and location after brain insult (Hu et al., 2015; Skaper et al., 2012), the increase in MD in voxels with a co-localized elevation in [^{11}C]PBR28 binding suggests that glial activation may be associated with net loss in tissue microstructure in chronic stroke patients. This rise in MD might reflect phagocytosis by activated glia to clear debris generated by stroke-induced secondary neurodegeneration. As chronically activated glia may have neurotoxic effects due to constitutive secretion of pro-inflammatory cytokines and other cytotoxic factors (Block et al., 2007), it is also possible that the rise in MD reflects progressive neurodegeneration due to neurotoxic activity of chronic glial activation in the stroke patients.

The current study has some limitations. First, the patient sample size was relatively small, in part because we required a specific stroke territory (MCA) and relatively narrow window of stroke chronicity (1–3 years). While these inclusion criteria increased patient homogeneity and thereby aided data interpretation, the patient cohort was too small to validly test associations between neuroinflammation and clinical characteristics such as fatigue and depression. Future [^{11}C]PBR28 PET studies with a large patient group is warranted in order to understand the clinical significance of neuroinflammation in chronic stroke patients. The patient group happened to have relatively few females (1/8), which while not statistically different from the proportion of females in the control group, might have affected the magnitude of group difference in [^{11}C]PBR28 binding. However, recent studies suggest that TSPO binding availability (Tuisku et al., 2019) and TSPO binding in response to a pro-inflammatory challenge (Murtaj et al., 2019) might be higher in females than males, leading to the possibility that [^{11}C]PBR28 binding in stroke patients relative to controls might be more elevated than observed in this pilot study. A second limitation is that to reduce the burden to patients, we used a semi-quantitative ratio metric of [^{11}C]PBR28 binding (SUVR) rather than quantitative kinetic modeling that relies on repeated arterial blood sampling. While kinetic modeling is considered the gold standard for quantifying TSPO binding, the validity of [^{11}C]PBR28 SUVR as a metric for glial activation is supported by a growing number of studies (Albrecht et al., 2018; Alshelh et al., 2020; Herranz et al., 2016; Van Weehaeghe et al., 2020). Third, while elevated TSPO binding is a well recognized marker of neuroinflammation, it is possible that increased uptake of the radioligand across the blood-brain-barrier contributed to the elevated [^{11}C]PBR28 binding in our patients. However, since neuroinflammation often causes changes in blood-brain-barrier permeability (Albrecht et al., 2016), an increase in [^{11}C]PBR28 brain uptake would not invalidate our conclusion that neuroinflammation is present in patients with chronic MCA stroke. Fourth, while we detected group differences in MD and FA, our use of high b-value diffusion-weighting likely induced some non-Gaussian diffusion effects that were not well accounted for by the diffusion tensor model. And fifth, the patients had a higher incidence of some stroke risk factors than controls, which could have affected the magnitude of group differences in glial activation and diffusion abnormalities. Future studies should consider enrolling as controls persons with a history of transient ischemic attack, a cohort that would be expected to have stroke risk factors at the same frequency as stroke patients.

In conclusion, this pilot study is the first to demonstrate extensive neuroinflammation in a cohort of patients with chronic MCA stroke. Future longitudinal studies will be required to determine whether neuroinflammation in stroke patients plays a causal role in the development of secondary poststroke pathologies such as fatigue, depression and accelerated cognitive decline.

Declarations of interest

None.

Funding

1R21-NS110982-01 (JDS, MLL); DoD-W81XWH-14-1-0543 (MLL); R01-NS094306-01A1 (MLL); and R21-NS087472-01A1 (MLL)

Declaration of competing interest

The authors of this manuscript have no competing interest, including no financial interest or personal relationship, that has influenced the scientific integrity of this research study.

Acknowledgments

The authors thank Grae Arabasz, Shirley Hsu and Regan Butterfield for technical support, and Dr. Jennifer McNab for creating the diffusion sequence used in this study.

References

Albrecht, D.S., Granziera, C., Hooker, J.M., Loggia, M.L., 2016. In vivo imaging of human neuroinflammation. ACS Chem. Neurosci. 7, 470–483.
Albrecht, D.S., Normandin, M.D., Shcherbinin, S., Wooten, D.W., Schwarz, A.J., Zurcher, N.R., Barth, V.N., Guehl, N.J., Akeju, O., Atassi, N., Veronese, M., Turkheimer, F., Hooker, J.M., Loggia, M.L., 2018. Pseudoreference regions for glial imaging with (11)C-PBR28: investigation in 2 clinical cohorts. J. Nucl. Med. 59, 107–114.
Alshelh, Z., Albrecht, D.S., Bergan, C., Akeju, O., Clauw, D.J., Conboy, L., Edwards, R.R., Kim, M., Lee, Y.C., Protsenko, E., Napadow, V., Sullivan, K., Loggia, M.L., 2020. In-vivo imaging of neuroinflammation in veterans with Gulf War illness. Brain Behav. Immun. 87, 498–507.
Arlicot, N., Petit, E., Katsifis, A., Toutain, J., Divoux, D., Bodard, S., Roussel, S., Guilloteau, D., Bernaudin, M., Chalon, S., 2010. Detection and quantification of remote microglial activation in rodent models of focal ischaemia using the TSPO radioligand CLINDE. Eur. J. Nucl. Med. Mol. Imag. 37, 2371–2380.
Assaf, Y., Cohen, Y., 2000. Assignment of the water slow-diffusing component in the central nervous system using q-space diffusion MRS: implications for fiber tract imaging. Magn. Reson. Med. 43, 191–199.
Assaf, Y., Mayk, A., Eliash, S., Speiser, Z., Cohen, Y., 2003. Hypertension and neuronal degeneration in excised rat spinal cord studied by high-b value q-space diffusion magnetic resonance imaging. Exp. Neurol. 184, 726–736.
Barritt, A.W., Smithard, D.G., 2011. Targeting fatigue in stroke patients. ISRN Neurol 2011, 805646.

Basser, P.J., Pierpaoli, C., 1996. Microstructural and physiological features of tissues elucidated by quantitative-diffusion-tensor MRI. J. Magn. Reson. B 111, 209–219.
Baumann, P.S., Cammoun, L., Conus, P., Do, K.Q., Marquet, P., Meskaldji, D., Meuli, R., Thiran, J.P., Hagmann, P., 2012. High b-value diffusion-weighted imaging: a sensitive method to reveal white matter differences in schizophrenia. Psychiatr. Res. 201, 144–151.
Block, M.L., Zecca, L., Hong, J.S., 2007. Microglia-mediated neurotoxicity: uncovering the molecular mechanisms. Nat. Rev. Neurosci. 8, 57–69.
Brett, M., Leff, A.P., Rorden, C., Ashburner, J., 2001. Spatial normalization of brain images with focal lesions using cost function masking. Neuroimage 14, 486–500.
Briard, E., Zoghbi, S.S., Imaizumi, M., Gourley, J.P., Shetty, H.U., Hong, J., Cropley, V., Fujita, M., Innis, R.B., Pike, V.W., 2008. Synthesis and evaluation in monkey of two sensitive 11C-labeled aryloxyanilide ligands for imaging brain peripheral benzodiazepine receptors in vivo. J. Med. Chem. 51, 17–30.
Brott, T., Adams, H.P., Olinger, C.P., Marler, J.R., G, B.W., Biller, J., Spilker, J., Holleran, R., Eberle, R., Hertzberg, V., Rorick, M., Moonaw, C.J., M W, 1989. Measurements of acute cerebral infarction: a clinical examination scale. Stroke 20, 864–870.
Bruno, A., Akinwuntan, A.E., Lin, C., Close, B., Davis, K., Baute, V., Aryal, T., Brooks, D., Hess, D.C., Switzer, J.A., Nichols, F.T., 2011. Simplified modified rankin scale questionnaire: reproducibility over the telephone and validation with quality of life. Stroke 42, 2276–2279.
Buffon, F., Molko, N., Herve, D., Porcher, R., Denghien, I., Pappata, S., Le Bihan, D., Bousser, M.G., Chabriat, H., 2005. Longitudinal diffusion changes in cerebral hemispheres after MCA infarcts. J. Cerebr. Blood Flow Metabol. 25, 641–650.
Cox, S.R., Lyall, D.M., Ritchie, S.J., Bastin, M.E., Harris, M.A., Buchanan, C.R., Fawns-Ritchie, C., Barbu, M.C., de Nooij, L., Reus, L.M., Alloza, C., Shen, X., Neilson, E., Alderson, H.L., Hunter, S., Liewald, D.C., Whalley, H.C., McIntosh, A.M., Lawrie, S.M., Pell, J.P., Tucker-Drob, E.M., Wardlaw, J.M., Gale, C.R., Deary, I.J., 2019. Associations between vascular risk factors and brain MRI indices in UK Biobank. Eur. Heart J. 40, 2290–2300.
Egorova, N., Gottlieb, E., Khlif, M.S., Spratt, N.J., Brodtmann, A., 2019. Choroid plexus volume after stroke. Int. J. Stroke 14, 923–930.
Flansbjer, U.B., Holmb√§ck, A.M., Downham, D., Patten, C., Lexell, J., 2005. Reliability of gait performance tests in men and women with hemiparesis after stroke. J. Rehabil. Med. 37, 75–82.
Fukutomi, H., Glasser, M.F., Murata, K., Akasaka, T., Fujimoto, K., Yamamoto, T., Autio, J.A., Okada, T., Togashi, K., Zhang, H., Van Essen, D.C., Hayashi, T., 2019. Diffusion tensor model links to neurite orientation dispersion and density imaging at high b-value in cerebral cortical gray matter. Sci. Rep. 9, 12246.
Gerhard, A., Schwarz, J., Myers, R., Wise, R., Banati, R.B., 2005. Evolution of microglial activation in patients after ischemic stroke: a [11C](R)-PK11195 PET study. Neuroimage 24, 591–595.
Gons, R.A., de Laat, K.F., van Norden, A.G., van Oudheusden, L.J., van Uden, I.W., Norris, D.G., Zwiers, M.P., de Leeuw, F.E., 2010. Hypertension and cerebral diffusion tensor imaging in small vessel disease. Stroke 41, 2801–2806.
Gulyas, B., Toth, M., Schain, M., Airaksinen, A., Vas, A., Kostulas, K., Lindstrom, P., Hillert, J., Halldin, C., 2012. Evolution of microglial activation in ischaemic core and peri-infarct regions after stroke: a PET study with the TSPO molecular imaging biomarker [11C]vinpocetine. J. Neurol. Sci. 320, 110–117.
Gupta, R.K., Saksena, S., Hasan, K.M., Agarwal, A., Haris, M., Pandey, C.M., Narayana, P.A., 2006. Focal Wallerian degeneration of the corpus callosum in large middle cerebral artery stroke: serial diffusion tensor imaging. J. Magn. Reson. Imag. 24, 549–555.
Hagmann, P., Sporns, O., Madan, N., Cammoun, L., Pienaar, R., Wedeen, V.J., Meuli, R., Thiran, J.P., Grant, P.E., 2010. White matter maturation reshapes structural connectivity in the late developing human brain. Proc. Natl. Acad. Sci. U. S. A. 107, 19067–19072.
Herranz, E., Gianni, C., Louapre, C., Treaba, C.A., Govindarajan, S.T., Ouellette, R., Loggia, M.L., Sloane, J.A., Madigan, N., Izquierdo-Garcia, D., Ward, N., Mangeat, G., Granberg, T., Klawiter, E.C., Catana, C., Hooker, J.M., Taylor, N., Ionete, C., Kinkel, R.P., Mainero, C., 2016. Neuroinflammatory component of gray matter pathology in multiple sclerosis. Ann. Neurol. 80, 776–790.
Herve, D., Molko, N., Pappata, S., Buffon, F., LeBihan, D., Bousser, M.G., Chabriat, H., 2005. Longitudinal thalamic diffusion changes after middle cerebral artery infarcts. J. Neurol. Neurosurg. Psychiatry 76, 200–205.
Hu, X., Leak, R.K., Shi, Y., Suenaga, J., Gao, Y., Zheng, P., Chen, J., 2015. Microglial and macrophage polarization-new prospects for brain repair. Nat. Rev. Neurol. 11, 56–64.
Hughes, J.L., Jones, P.S., Beech, J.S., Wang, D., Menon, D.K., Aigbirhio, F.I., Fryer, T.D., Baron, J.C., 2012. A microPET study of the regional distribution of [11C]-PK11195 binding following temporary focal cerebral ischemia in the rat. Correlation with post mortem mapping of microglia activation. Neuroimage 59, 2007–2016.
Hyare, H., Thornton, J., Stevens, J., Mead, S., Rudge, P., Collinge, J., Yousry, T.A., Jager, H.R., 2010. High-b-value diffusion MR imaging and basal nuclei apparent diffusion coefficient measurements in variant and sporadic Creutzfeldt-Jakob disease. AJNR Am J Neuroradiol 31, 521–526.
Izquierdo-Garcia, D., Hansen, A.E., Forster, S., Benoit, D., Schachoff, S., Furst, S., Chen, K.T., Chonde, D.B., Catana, C., 2014. An SPM8-based approach for attenuation correction combining segmentation and nonrigid template formation: application to simultaneous PET/MR brain imaging. J. Nucl. Med. 55, 1825–1830.
Jason, E., Dastidar, P., Kalliokoski, A., Luukkaala, T., Soimakallio, S., 2011. Diffusion tensor imaging of chronic right cerebral hemisphere infarctions. J. Neuroimaging 21, 325–331.
Justicia, C., Ramos-Cabrer, P., Hoehn, M., 2008. MRI detection of secondary damage after stroke: chronic iron accumulation in the thalamus of the rat brain. Stroke 39, 1541–1547.
Kennedy, K.M., Raz, N., 2009. Pattern of normal age-related regional differences in white matter microstructure is modified by vascular risk. Brain Res. 1297, 41–56.
Kolb, A., Wehrl, H.F., Hofmann, M., Judenhofer, M.S., Eriksson, L., Ladebeck, R., Lichy, M.P., Byars, L., Michel, C., Schlemmer, H.P., Schmand, M., Claussen, C.D., Sossi, V., Pichler, B.J., 2012. Technical performance evaluation of a human brain PET/MRI system. Eur. Radiol. 22, 1776–1788.
Kreisl, W.C., Fujita, M., Fujimura, Y., Kimura, N., Jenko, K.J., Kannan, P., Hong, J., Morse, C.L., Zoghbi, S.S., Gladding, R.L., Jacobson, S., Oh, U., Pike, V.W., Innis, R.B., 2010. Comparison of [11C]-(R)-PK 11195 and [11C]PBR28, two radioligands for translocator protein (18 kDa) in human and monkey: implications for positron emission tomographic imaging of this inflammation biomarker. Neuroimage 49, 2924–2932.
Kuchcinski, G., Munsch, F., Lopes, R., Bigourdan, A., Su, J., Sagnier, S., Renou, P., Pruvo, J.P., Rutt, B.K., Dousset, V., Sibon, I., Tourdias, T., 2017. Thalamic alterations remote to infarct appear as focal iron accumulation and impact clinical outcome. Brain 140, 1932–1946.
Liang, Z., Zeng, J., Liu, S., Ling, X., Xu, A., Yu, J., Ling, L., 2007. A prospective study of secondary degeneration following subcortical infarction using diffusion tensor imaging. J. Neurol. Neurosurg. Psychiatry 78, 581–586.
Loggia, M.L., Chonde, D.B., Akeju, O., Arabasz, G., Catana, C., Edwards, R.R., Hill, E., Hsu, S., Izquierdo-Garcia, D., Ji, R.R., Riley, M., Wasan, A.D., Zurcher, N.R., Albrecht, D.S., Vangel, M.G., Rosen, B.R., Napadow, V., Hooker, J.M., 2015. Evidence for brain glial activation in chronic pain patients. Brain 138, 604–615.
Maclullich, A.M., Ferguson, K.J., Reid, L.M., Deary, I.J., Starr, J.M., Seckl, J.R., Bastin, M.E., Wardlaw, J.M., 2009. Higher systolic blood pressure is associated with increased water diffusivity in normal-appearing white matter. Stroke 40, 3869–3871.
Maillard, P., Seshadri, S., Beiser, A., Himali, J.J., Au, R., Fletcher, E., Carmichael, O., Wolf, P.A., DeCarli, C., 2012. Effects of systolic blood pressure on white-matter integrity in young adults in the Framingham Heart Study: a cross-sectional study. Lancet Neurol. 11, 1039–1047.
McEvoy, L.K., Fennema-Notestine, C., Eyler, L.T., Franz, C.E., Hagler Jr., D.J., Lyons, M.J., Panizzon, M.S., Rinker, D.A., Dale, A.M., Kremen, W.S., 2015. Hypertension-related alterations in white matter microstructure detectable in middle age. Hypertension 66, 317–323.
Middleton, A., Fritz, S.L., Lusardi, M., 2015. Walking speed: the functional vital sign. J. Aging Phys. Activ 23, 314–322.
Morris, R.S., Simon Jones, P., Alawneh, J.A., Hong, Y.T., Fryer, T.D., Aigbirhio, F.I., Warburton, E.A., Baron, J.C., 2018. Relationships between selective neuronal loss and microglial activation after ischaemic stroke in man. Brain May 9.
Murtaj, V., Belloli, S., Di Grigoli, G., Pannese, M., Ballarini, E., Rodriguez-Menendez, V., Marmiroli, P., Cappelli, A., Masiello, V., Monterisi, C., Bellelli, G., Panina-Bordignon, P., Moresco, R.M., 2019. Age and sex influence the neuro-inflammatory response to a peripheral acute LPS challenge. Front. Aging Neurosci. 11, 299.
Myers, R., Manjil, L.G., Cullen, B.M., Price, G.W., Frackowiak, R.S., Cremer, J.E., 1991a. Macrophage and astrocyte populations in relation to [3H]PK 11195 binding in rat cerebral cortex following a local ischaemic lesion. J. Cerebr. Blood Flow Metabol. 11, 314–322.
Myers, R., Manjil, L.G., Frackowiak, R.S., Cremer, J.E., 1991b. [3H]PK 11195 and the localisation of secondary thalamic lesions following focal ischaemia in rat motor cortex. Neurosci. Lett. 133, 20–24.
Nowicka, D., Rogozinska, K., Aleksy, M., Witte, O.W., Skangiel-Kramska, J., 2008. Spatiotemporal dynamics of astroglial and microglial responses after photothrombotic stroke in the rat brain. Acta Neurobiol. Exp. 68, 155–168.
Ogawa, T., Yoshida, Y., Okudera, T., Noguchi, K., Kado, H., Uemura, K., 1997. Secondary thalamic degeneration after cerebral infarction in the middle cerebral artery distribution: evaluation with MR imaging. Radiology 204, 255–262.
Owen, D.R., Yeo, A.J., Gunn, R.N., Song, K., Wadsworth, G., Lewis, A., Rhodes, C., Pulford, D.J., Bennacef, I., Parker, C.A., StJean, P.L., Cardon, L.R., Mooser, V.E., Matthews, P.M., Rabiner, E.A., Rubio, J.P., 2012. An 18-kDa translocator protein (TSPO) polymorphism explains differences in binding affinity of the PET radioligand PBR28. J. Cerebr. Blood Flow Metabol. 32, 1–5.
Pappata, S., Levasseur, M., Gunn, R.N., Myers, R., Crouzel, C., Syrota, A., Jones, T., Kreutzberg, G.W., Banati, R.B., 2000. Thalamic microglial activation in ischemic stroke detected in vivo by PET and [11C]PK1195. Neurology 55, 1052–1054.
Price, C.J., Wang, D., Menon, D.K., Guadagno, J.V., Cleij, M., Fryer, T., Aigbirhio, F., Baron, J.C., Warburton, E.A., 2006. Intrinsic activated microglia map to the peri-infarct zone in the subacute phase of ischemic stroke. Stroke 37, 1749–1753.
Radlinska, B.A., Ghinani, S.A., Lyon, P., Jolly, D., Soucy, J.P., Minuk, J., Schirrmacher, R., Thiel, A., 2009. Multimodal microglia imaging of fiber tracts in acute subcortical stroke. Ann. Neurol. 66, 825–832.
Reas, E.T., Hagler Jr., D.J., Andrews, M.J., Lee, R.R., Dale, A.M., McEvoy, L.K., 2020. Associations between age and brain microstructure in older community-dwelling men and women: the Rancho Bernardo Study. Neurobiol. Aging 95, 94–103.
Rojas, S., Martin, A., Arranz, M.J., Pareto, D., Purroy, J., Verdaguer, E., Llop, J., Gomez, V., Gispert, J.D., Millan, O., Chamorro, A., Planas, A.M., 2007. Imaging brain inflammation with [(11)C]PK11195 by PET and induction of the peripheral-type benzodiazepine receptor after transient focal ischemia in rats. J. Cerebr. Blood Flow Metabol. 27, 1975–1986.
Salat, D.H., Tuch, D.S., Greve, D.N., van der Kouwe, A.J., Hevelone, N.D., Zaleta, A.K., Rosen, B.R., Fischl, B., Corkin, S., Rosas, H.D., Dale, A.M., 2005. Age-related alterations in white matter microstructure measured by diffusion tensor imaging. Neurobiol. Aging 26, 1215–1227.
Salat, D.H., Williams, V.J., Leritz, E.C., Schnyer, D.M., Rudolph, J.L., Lipsitz, L.A., McGlinchey, R.E., Milberg, W.P., 2012. Inter-individual variation in blood pressure is associated with regional white matter integrity in generally healthy older adults. Neuroimage 59, 181–192.

Salminen, L.E., Conturo, T.E., Laidlaw, D.H., Cabeen, R.P., Akbudak, E., Lane, E.M., Heaps, J.M., Bolzenius, J.D., Baker, L.M., Cooley, S., Scott, S., Cagle, L.M., Phillips, S., Paul, R.H., 2016. Regional age differences in gray matter diffusivity among healthy older adults. Brain Imaging Behav 10, 203–211.

Schroeter, M., Jander, S., Witte, O.W., Stoll, G., 1999. Heterogeneity of the microglial response in photochemically induced focal ischemia of the rat cerebral cortex. Neuroscience 89, 1367–1377.

Sette, G., Baron, J.C., Young, A.R., Miyazawa, H., Tillet, I., Barre, L., Travere, J.M., Derlon, J.M., MacKenzie, E.T., 1993. In vivo mapping of brain benzodiazepine receptor changes by positron emission tomography after focal ischemia in the anesthetized baboon. Stroke 24, 2046–2057 discussion 2057-2048.

Shi, K., Tian, D.C., Li, Z.G., Ducruet, A.F., Lawton, M.T., Shi, F.D., 2019. Global brain inflammation in stroke. Lancet Neurol. 18, 1058–1066.

Shiraishi, A., Hasegawa, Y., Okada, S., Kimura, K., Sawada, T., Mizusawa, H., Minematsu, K., 2005. Highly diffusion-sensitized tensor imaging of unilateral cerebral arterial occlusive disease. AJNR Am J Neuroradiol 26, 1498–1504.

Skaper, S.D., Giusti, P., Facci, L., 2012. Microglia and mast cells: two tracks on the road to neuroinflammation. Faseb. J. 26, 3103–3117.

Smets, E.M., Garssen, B., Bonke, B., De Haes, J.C., 1995. The Multidimensional Fatigue Inventory (MFI) psychometric qualities of an instrument to assess fatigue. J. Psychosom. Res. 39, 315–325.

Smith, S.M., Nichols, T.E., 2009. Threshold-free cluster enhancement: addressing problems of smoothing, threshold dependence and localisation in cluster inference. Neuroimage 44, 83–98.

Spalletta, G., Bossu, P., Ciaramella, A., Bria, P., Caltagirone, C., Robinson, R.G., 2006. The etiology of poststroke depression: a review of the literature and a new hypothesis involving inflammatory cytokines. Mol. Psychiatr. 11, 984–991.

Taniwaki, Y., Kato, M., Araki, T., Kobayashi, T., 1996. Microglial activation by epileptic activities through the propagation pathway of kainic acid-induced hippocampal seizures in the rat. Neurosci. Lett. 217, 29–32.

Thiel, A., Radlinska, B.A., Paquette, C., Sidel, M., Soucy, J.P., Schirrmacher, R., Minuk, J., 2010. The temporal dynamics of poststroke neuroinflammation: a longitudinal diffusion tensor imaging-guided PET study with 11C-PK11195 in acute subcortical stroke. J. Nucl. Med. 51, 1404–1412.

Topper, R., Gehrmann, J., Schwarz, M., Block, F., Noth, J., Kreutzberg, G.W., 1993. Remote microglial activation in the quinolinic acid model of Huntington's disease. Exp. Neurol. 123, 271–283.

Tuisku, J., Plaven-Sigray, P., Gaiser, E.C., Airas, L., Al-Abdulrasul, H., Bruck, A., Carson, R.E., Chen, M.K., Cosgrove, K.P., Ekblad, L., Esterlis, I., Farde, L., Forsberg, A., Halldin, C., Helin, S., Kosek, E., Lekander, M., Lindgren, N., Marjamaki, P., Rissanen, E., Sucksdorff, M., Varrone, A., , HRRT [11C]PBR study group, Collste, K., Gallezot, J.D., Hillmer, A., Huang, Y., Hoglund, C.O., Johansson, J., Jucaite, A., Lampa, J., Nabulsi, N., Pittman, B., Sandiego, C.M., Stenkrona, P., Rinne, J., Matuskey, D., Cervenka, S., 2019. Effects of age, BMI and sex on the glial cell marker TSPO - a multicentre [(11)C]PBR28 HRRT PET study. Eur. J. Nucl. Med. Mol. Imag. 46, 2329–2338.

Van Weehaeghe, D., Babu, S., De Vocht, J., Zurcher, N.R., Chew, S., Tseng, C.J., Loggia, M.L., Koole, M., Rezaei, A., Schramm, G., Van Damme, P., Hooker, J.M., Van Laere, K., Atassi, N., 2020. Moving toward multicenter therapeutic trials in Amyotrophic Lateral Sclerosis: feasibility of data pooling using different translocator protein PET radioligands. J. Nucl. Med. 61, 1621–1627.

Vogt, N.M., Hunt, J.F., Adluru, N., Dean, D.C., Johnson, S.C., Asthana, S., Yu, J.J., Alexander, A.L., Bendlin, B.B., 2020. Cortical microstructural alterations in mild cognitive impairment and Alzheimer's disease dementia. Cerebr. Cortex 30, 2948–2960.

Walberer, M., Jantzen, S.U., Backes, H., Rueger, M.A., Keuters, M.H., Neumaier, B., Hoehn, M., Fink, G.R., Graf, R., Schroeter, M., 2014. In-vivo detection of inflammation and neurodegeneration in the chronic phase after permanent embolic stroke in rats. Brain Res. 1581, 80–88.

Walter, H.L., Walberer, M., Rueger, M.A., Backes, H., Wiedermann, D., Hoehn, M., Neumaier, B., Graf, R., Fink, G.R., Schroeter, M., 2015. In vivo analysis of neuroinflammation in the late chronic phase after experimental stroke. Neuroscience 292, 71–80.

Werring, D.J., Toosy, A.T., Clark, C.A., Parker, G.J., Barker, G.J., Miller, D.H., Thompson, A.J., 2000. Diffusion tensor imaging can detect and quantify corticospinal tract degeneration after stroke. J. Neurol. Neurosurg. Psychiatry 69, 269–272.

Woodbury, M.L., Velozo, C.A., Richards, L.G., Duncan, P.W., Studenski, S., Lai, S.M., 2007. Dimensionality and construct validity of the Fugl-Meyer Assessment of the upper extremity. Arch. Phys. Med. Rehabil. 88, 715–723.

Yoshiura, T., Mihara, F., Tanaka, A., Ogomori, K., Ohyagi, Y., Taniwaki, T., Yamada, T., Yamasaki, T., Ichimiya, A., Kinukawa, N., Kuwabara, Y., Honda, H., 2003. High b value diffusion-weighted imaging is more sensitive to white matter degeneration in Alzheimer's disease. Neuroimage 20, 413–419.

Zigmond, A.S., Snaith, R.P., 1983. The hospital anxiety and depression scale. Acta Psychiatr. Scand. 67, 361–370.